

Electronic detection of surface plasmon polaritons by metal-oxide-silicon capacitor

Robert E. Peale, Evan Smith, Christian W. Smith, Farnood Khalilzadeh-Rezaie, Masa Ishigami, Nima Nader, Shiva Vangala, and Justin W. Cleary

Citation: *APL Photonics* **1**, 066103 (2016); doi: 10.1063/1.4962428

View online: <http://dx.doi.org/10.1063/1.4962428>

View Table of Contents: <http://scitation.aip.org/content/aip/journal/app/1/6?ver=pdfcov>

Published by the [AIP Publishing](#)

Articles you may be interested in

[A silicon-on-insulator surface plasmon interferometer for hydrogen detection](#)

J. Appl. Phys. **120**, 043106 (2016); 10.1063/1.4959261

[Fano response induced by the interference between localized plasmons and interface reflections in metal-insulator-metal waveguide structure](#)

J. Appl. Phys. **119**, 243101 (2016); 10.1063/1.4953682

[Surface plasmon polariton excitation by electrostatic modulation and phase grating in indium-tin-oxide coated lithium niobate slabs](#)

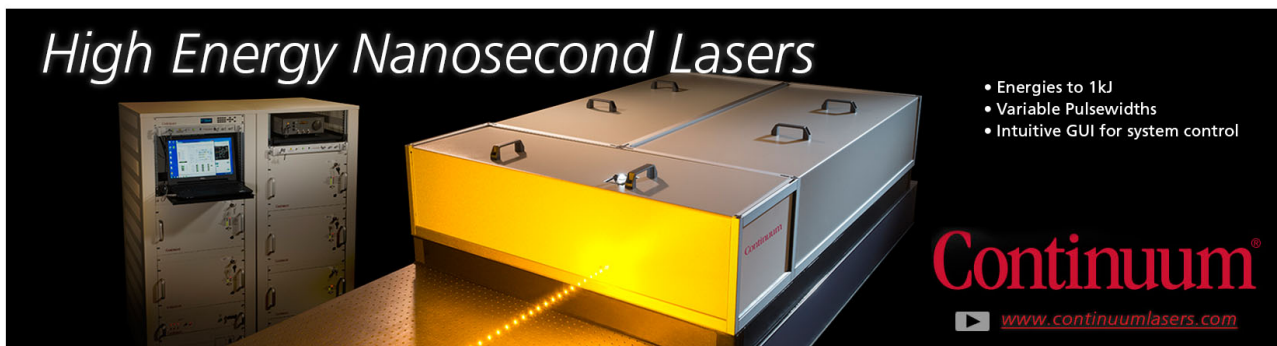
J. Appl. Phys. **118**, 063102 (2015); 10.1063/1.4928611

[Excitations of surface plasmon polaritons in double layer metal grating structures](#)

Appl. Phys. Lett. **100**, 091111 (2012); 10.1063/1.3690947

[Broadband high-efficiency surface-plasmon-polariton coupler with silicon-metal interface](#)

Appl. Phys. Lett. **95**, 013504 (2009); 10.1063/1.3168653



High Energy Nanosecond Lasers

- Energies to 1kJ
- Variable Pulsewidths
- Intuitive GUI for system control

Continuum[®]

www.continuumlasers.com

Electronic detection of surface plasmon polaritons by metal-oxide-silicon capacitor

Robert E. Peale,¹ Evan Smith,^{2,3} Christian W. Smith,¹
 Farnood Khalilzadeh-Rezaie,¹ Masa Ishigami,¹ Nima Nader,^{2,3}
 Shiva Vangala,^{2,4} and Justin W. Cleary²

¹Department of Physics, University of Central Florida, Orlando, Florida 32816, USA

²Air Force Research Laboratory, Sensors Directorate, 2241 Avionics Circle, Wright-Patterson Air Force Base, Ohio 45433, USA

³Wyle Laboratories, 2601 Mission Point Blvd., Dayton, Ohio 45431, USA

⁴SURVICE Engineering, 4141 Colonel Glenn Hwy, Dayton, Ohio 45431, USA

(Received 7 June 2016; accepted 28 August 2016; published online 20 September 2016)

An electronic detector of surface plasmon polaritons (SPPs) is reported. SPPs optically excited on a metal surface using a prism coupler are detected by using a close-coupled metal-oxide-silicon (MOS) capacitor. Incidence-angle dependence is explained by Fresnel transmittance calculations, which also are used to investigate the dependence of photo-response on structure dimensions. Electrodynamic simulations agree with theory and experiment and additionally provide spatial intensity distributions on and off the SPP excitation resonance. Experimental dependence of the photoresponse on substrate carrier type, carrier concentration, and back-contact biasing is qualitatively explained by simple theory of MOS capacitors. © 2016 Author(s). All article content, except where otherwise noted, is licensed under a Creative Commons Attribution (CC BY) license (<http://creativecommons.org/licenses/by/4.0/>). [<http://dx.doi.org/10.1063/1.4962428>]

Surface plasmon polaritons (SPPs) are electromagnetic waves bound to the surface of a conductor. SPP fields decay exponentially into the dielectric medium above the surface. Direct detection schemes for SPPs have recently been reviewed.¹ Of particular note are devices comprising an Otto coupler,² in which a prism allows excitation of an SPP directly on a nearby metal, and where this metal is a semi-transparent metal contact of a photodetector, such as a Schottky diode.³ The fields of this SPP induce internal photoemission of hot-carriers within the contact metal, or they penetrate the semiconductor to excite electron hole pairs, which are electrically detected. Here, we present the detection of SPPs on the metal layer of a Kretschmann prism-coupler⁴ by bringing a metal-oxide-silicon (MOS)-capacitor into proximity of the SPP fields.

Electrical sensing of SPPs by a close-coupled photocapacitor comprising transparent conductor, dielectric, and semiconductor has been described in our preliminary reports.^{5,6} The sign of the transient photocurrent depends on carrier type, the photoresponse is maximum at intermediate resistivity values, and the response can be amplified or extinguished by suitable substrate bias. Combined angle- and wavelength-dependence for resonant excitation of surface plasmons suggests applications to spectral sensing and imaging.

Fig. 1 presents a schematic of our experiment. Electromagnetic radiation is internally incident on a thin metal film on the long face of a Kretschmann prism coupler,⁴ where SPPs are excited at a particular frequency determined by the internal incidence angle. In usual Kretschmann couplers, SPPs are excited beyond the total internal reflection angle, so that no light is transmitted into free space beyond the metal coated surface of the prism. However, in our device a photocapacitor is close coupled to the active prism surface via a sub-micron air gap, so that it is able to “pick-off” some of the evanescent fields of the SPP in a process similar to frustrated total internal reflection. However, because there is a transparent conductor on the top surface of the close-coupled photocapacitor, the device might be better described as a hybrid Kretschmann-Otto coupler. In the Kretschmann coupler, the SPP lives on a thin layer of metal on the prism. In the Otto coupler,² the



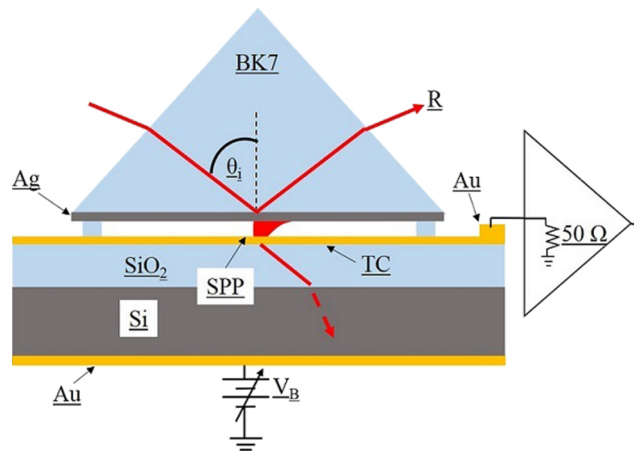


FIG. 1. Device schematic. The width of the shaded region in the air-gap represents field intensity associated with a surface plasmon polariton that is bound primarily to the Ag surface.

SPP lives on the metal surface that is separated by an air gap from a bare prism. In the hybrid structure, the SPP might be shared between both metal layers. This situation is suggested by the intensity distribution in the schematic air gap, where most of the SPP is on the Ag layer, while less of the SPP exists on the Au layer. Our Au layer is thin enough for light to be transmitted through it, thence through the oxide, and finally into the silicon, where it is absorbed. The resulting photo-induced minority carriers are attracted by band-bending to the oxide-silicon interface, inducing a transient displacement current in the capacitor. This photocurrent is amplified by a current amplifier with internal $50\ \Omega$ input load resistance. DC biasing the blanket back contact changes the depletion width and band-bending, which amplifies or suppresses the photo current.

This paper explains and investigates the angle-dependent response spectrum. It reveals the intensity distribution in all layers, showing that the device is primarily of Kretschmann type. It presents and explains the dependence of the photoresponse on substrate carrier type, concentration, and biasing. The subject device is a plasmonic-to-electronic transducer, with potential application to proposed plasmonic integrated circuits and sensors. In particular, spectral sensing and imaging is a potential application, where different wavelength targets depend on choice of materials and SPP excitation methods.⁷⁻¹³

Fabrication details for Fig. 1 device have previously been published.^{5,6} The Ag/air/Au/thermal-oxide layers had nominal thicknesses 45/600/30/280 nm. The air-gap provides dielectric contrast necessary to excite SPPs, represented schematically in Fig. 1 by a decaying intensity distribution that extends into the silicon through semitransparent metal and oxide. An on-off modulated, TM-polarized, 651 nm wavelength laser is internally reflected from the metalized prism face at an internal incidence angle θ_i . Angular uncertainty is $\sim 0.3^\circ$. Displacement current in the capacitor is amplified by a current preamp.

Dependence of MOS photocurrent on substrate conductivity type, concentration, and biasing is investigated independently of the SPPs and prism coupler using a chopped HeNe laser at 632 nm wavelength. The chopped incident laser signal is sampled with a reference detector to verify the sign of the transient photocurrent. For these samples, oxide is either thermally grown with $1\ \mu\text{m}$ thickness, or plasma-enhanced-chemical-vapor-deposited (PECVD) with 280 nm thickness. The former allows larger substrate bias without leakage.

Theoretical angle-dependent transmittance into the silicon and reflectance from the layers is obtained from multilayer Fresnel calculations.¹⁴ Numerical values are calculated from the analytical formulas using Mathematica for the case of light that is TM-polarized, the necessary polarization for SPP excitation. The BK7 incidence medium and Si exit medium are taken to be semi-infinite. Complex permittivity values at 651 nm wavelength for BK7/Ag/air/Au/oxide/Si are taken to be $2.294/(-17.209 + 1.162i)/(-9.909 + 0.7308i)/2.122/(14.7992 + 0.123i)$. All values are from Palik,¹⁵ except for BK7 which is from the material data sheet.¹⁶

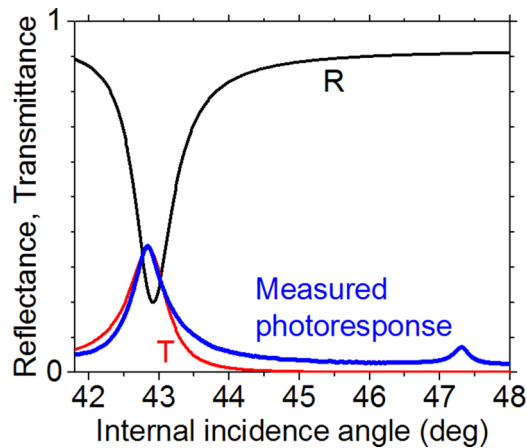


FIG. 2. Measured resonance detection of surface plasmon polariton by MOS photocapacitor compared with calculated transmittance and reflectance.

Fig. 2 presents measured photoresponse for the Fig. 1 device. The silicon substrate is p-type with resistivity 10-25 Ω -cm. When heavily doped substrate of <0.005 Ω -cm resistivity is used, there is no measurable photoresponse. The photoresponse curve is scaled to have the same magnitude as the calculated transmittance. The thicknesses of the metals, air gap, and oxide are manually adjusted in the calculation until there is reasonable match with the angular position and width of the measured resonance. The best choice of thicknesses in the calculation for the Ag/air/Au/oxide layers is 50/900/15/260 nm, which differs somewhat from their nominal values. These differences are within fabrication and measurement tolerances. Moreover, differences in permittivities for very thin metals from published bulk values¹⁷ may affect the best fit values of thicknesses for those films. The photocurrent peaks close to the SPP resonance angle defined by the minimum in the reflectance curve. The secondary measured peak at higher angles is due to back-reflection from the exit facet of the prism,⁶ since the two peaks are symmetric about 45° and converge to this angle as the wavelength is decreased.

The usual evidence for excitation of an SPP in a Kretschmann coupler is the reflection dip that appears above the critical angle, as shown in our Fig. 2. The characteristics of such dips have been amply explained in the literature in terms of SPP theory based on material permittivities, with emphasis placed on the in-plane-momentum-conserving coupling condition. However, it is important to note that the full reflectivity curve for Kretschmann couplers is always calculated with perfect accuracy using standard Fresnel formulas. In this sense, the excitation of the SPP might alternatively be described as a Fabry-Perot resonance inside the extremely lossy metal layer, with corresponding enhancement of the local intensity. That the calculated transmittance resonance, which corresponds to the similarly calculated SPP-identified reflectivity minimum, coincides with the photocurrent resonance is evidence that the photocurrent is generated by fields of the excited SPP.

Lumerical FDTD Solutions software is used to investigate the electrodynamic fields within the layer structure with these results being presented in Fig. 3. The dimensions and optical constants are taken to be the same as for the Fresnel calculations plotted in Fig. 2. The squared magnitude of the electric field is plotted as a function of position normal to the surfaces. Different angles of incidence θ_i are considered in steps of 0.02° . The curve for R vs. θ_i obtained from the simulation agrees perfectly with the curve in Fig. 2. The minimum in R is found at the resonance angle 42.98° , and the intensity distribution at this angle is plotted in Fig. 3. Also plotted are simulation results at 45° , which is well off resonance. A number of observations can be made in Fig. 3. The on-off resonance intensity ratio of ~ 2 for the near fields within the prism includes the incident wave, but the ratio of the intensity in the far fields (not shown) accurately reproduces the ratio in Fig. 2 reflectivity curve. There is strong attenuation within the metals, but the intensity is higher on resonance than off, especially on the air-gap side of the Ag layer. The intensity at the Ag-air

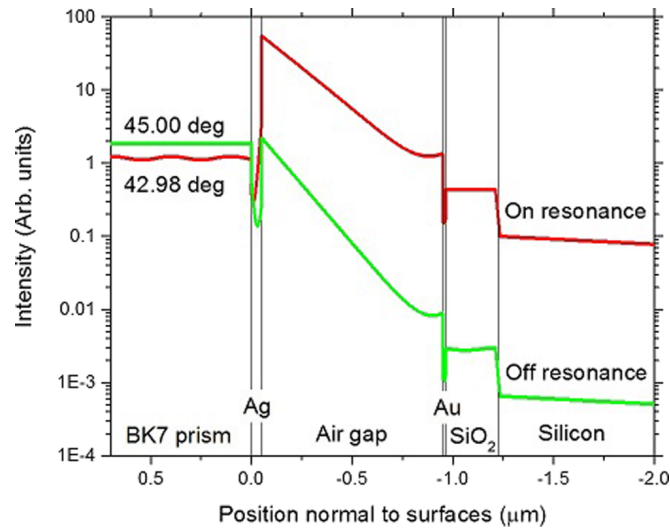


FIG. 3. Intensity distribution in device determined from electrodynamic simulations. Vertical lines indicate layer boundaries.

interface is $26\times$ larger on-resonance than off, a clear indication of the resonant excitation of an SPP, whose intensity decays exponentially across the air gap as it should. Only a slight upturn in the intensity is observed at the air-gold interface, showing that the Otto-coupling effect is very weak. In other words, our structure is best described as a Kretschmann coupler with a photo-capacitor that samples just the tail of the SPP intensity distribution and only slightly perturbs the SPP fields. The field that penetrates into the silicon is $\sim 150\times$ stronger on resonance than off. The silicon absorption coefficient determined from the decay is $0.32 \mu\text{m}^{-1}$ at $\lambda = 651 \text{ nm}$ wavelength, which agrees very well with the value $4\pi\kappa/\lambda$ determined from the published extinction coefficient κ .¹⁵

Fig. 4 presents a series of Fresnel calculations to reveal the effect of varying air gap and oxide thickness. Photocurrent is reasonably expected to be proportional to the transmittance into the silicon, where all transmitted light is absorbed. Thicknesses of Ag and Au layers are taken to be the best-fit values 50 and 15 nm, respectively. Resonances shift downward toward the surface plasmon resonance (SPR) angle of the simple prism coupler, and the resonance sharpens, as the air gap is increased. For the thicker oxide, multiple transmission peaks appear due to Fabry-Perot resonances, but these merge when the gap becomes as large as 800 nm. Transmittance is maximum at 900 nm air-gap for 300 nm oxide thickness. For larger air gaps, the photocapacitor feels less and less of the

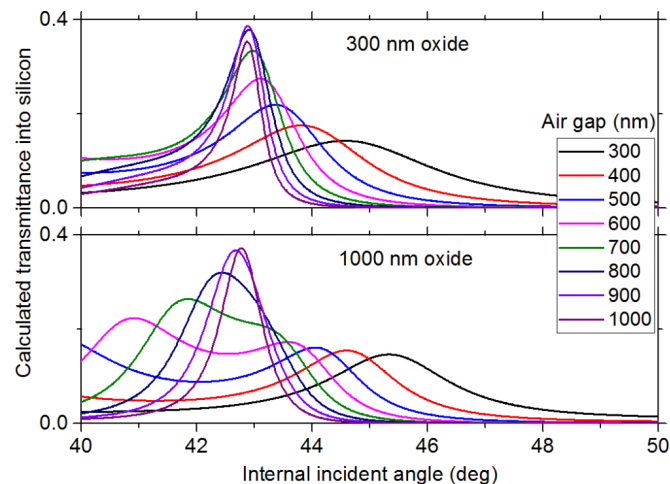


FIG. 4. Calculated transmittance resonances for different air gap and oxide thicknesses.

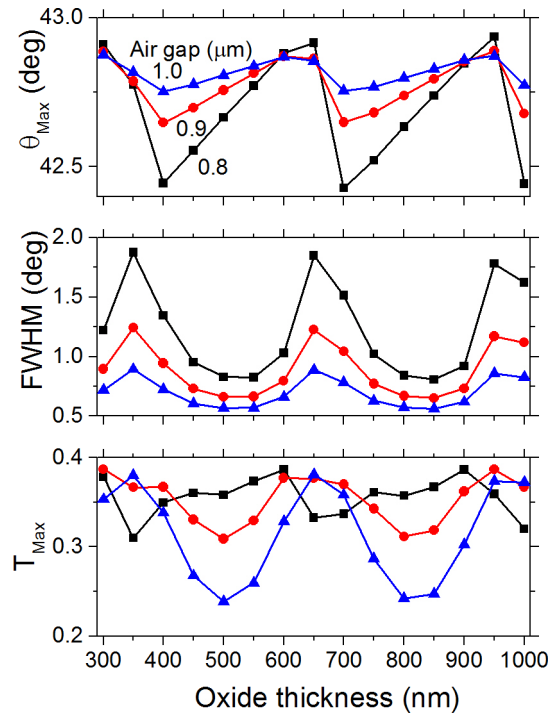


FIG. 5. Resonance angle, resonance full width at half maximum, and peak transmittance into silicon as a function of MOS oxide thickness for various air gaps between SPP prism coupler and MOS photocapacitor.

decaying tail of the SPP, and the peak decreases. For 1000 nm oxide, the peak is still growing at 1000 nm air gap because the two transmission resonances continue to merge. On the other hand, as the air gap is reduced below 900 nm, the transmission resonance gradually spreads out over a broader range of angles, and the peak transmittance becomes less. In other words, it gradually loses the character of a resonance. This is easy to understand, by considering the limit of zero air gap. Then the index discontinuity of the resulting prism/metal/silicon structure would have the wrong sign for the excitation of an SPP. There would be no total internal reflection, and transmission would be spread over all angles.

Fig. 5 presents calculated photoresponse resonance angle, resonance full width at half maximum (FWHM), and peak transmittance for various air gaps and oxide thicknesses. Results show that the angle for resonant photo response tends to oscillate by up to $\sim 0.5^\circ$ with changing oxide thickness. The phase of the oscillation is independent of air gap. The oscillation amplitude is smallest for larger air gaps. Since the air gap thickness has the highest uncertainty of all the layers due to the challenge of precisely mating prism to capacitor, larger gaps would be favorable for applications that require consistent resonance angle.

The full width at half maximum (FWHM) of the resonance also oscillates with gap-independent phase. The sharpest response resonances occur for the largest air gap, and for these the oscillation amplitude is smaller. Since sharp resonances are usually desirable for applications, this consideration also favors larger air gaps.

Peak transmittance is observed to oscillate between about 24% and 38% with changing oxide thickness. The phase of these oscillations here depends on the air-gap thickness. The minimum amplitude of the oscillation occurs for the smallest air gap, but there is hardly any dependence of the maximum transmittance on air gap for the range of gaps considered. Since it is easy to control oxide thickness, there is not much reason to favor small air gaps based on these transmission data. Strong photoresponse can be achieved with the larger air gap by carefully controlling the other layer thicknesses. On the other hand, Fig. 4 shows that the peak response will eventually decline as the MOS sensor is moved farther from the prism, due to the decay of the evanescent SPP fields. The

oscillations with oxide thickness observed in all three parts of Fig. 5 are not surprising, because the multi-layer structure consists of multiple Fabry-Perot cavities.

The observed photoresponse and dependence on doping sign, resistivity, and bias are qualitatively explained by the simplest MOS model.¹⁸ This model ignores non-idealities such as differences in metal and semiconductor work functions, oxide charges, interface traps, and induced charges. In particular, it assumes that flat band conditions occur at zero bias, which if true would mean no collected photocurrent in the absence of an applied bias, in contradiction to what we actually observe. Thus, this model is not expected to be quantitatively accurate, but it is instructive nevertheless.

First we note that the sign of the observed photocurrent is consistent with flow of photo-induced minority carriers toward the substrate/oxide interface. Namely, the photocurrent is negative for p-type and positive for n-type silicon.⁶ For example, electrons that are photo-generated within the depletion region under the metal top contact on p-Si are swept toward the contact by the electric field in the bent-band region.

The next observation is the dependence of photoresponse magnitude on doping level. The photoresponse is zero for low-resistivity substrates, strongest for intermediate resistivity, and very small for high resistivity.⁶ Minority carriers are photo-excited to a depth $\sim 1/\alpha$, where the absorption coefficient α for Si at 632 nm wavelength has the value $0.31 \mu\text{m}^{-1}$,¹⁵ giving an optical penetration depth of $\sim 3 \mu\text{m}$. Only those minority carriers generated within the depletion region, where there is band bending, contribute to photocurrent. The maximum possible depletion width W_T occurs at the threshold between depletion and inversion bias conditions, and W_T decreases as inverse square root of doping concentration (see Fig. 16.9 in Ref. 18). The heavily doped substrates investigated (1-7 m Ω -cm) have $W_T < 10 \text{ nm}$, which is 300 times smaller than the optical penetration. A reduction in the collection of photo-generated minority carriers by this factor puts the photoresponse below our noise level, in agreement with observations.

The low-doped samples studied had resistivity 3000 Ω -cm, for which W_T exceeds 20 μm , which is 6 \times more than the optical penetration depth. Thus, all of the photo-generated carriers are within the depletion width and would be collected, if there are no other factors at play. In fact we see only a very small signal for such lightly doped substrates. We suggest that the transient photocurrent is inversely proportional to capacitive reactance, i.e., it is proportional to capacitance C , which decreases with increasing W_T . Additionally, the finite minority-carrier diffusion length may limit collection of those carriers photo-generated far from the top contact.

Interestingly, for the studied samples with intermediate resistivity ($\sim 10 \Omega$ -cm), which gave strong photo-response, W_T is $\sim 1 \mu\text{m}$, which is just 3 \times smaller than the optical penetration depth. Based on the foregoing considerations, we might tentatively expect even stronger photo-response with a substrate resistivity closer to 100 Ω -cm.

We note that the actual depletion width W at zero applied bias should be less than W_T . In the over-simplified model considered in this discussion, zero bias implies flat-band conditions with $W = 0$, such that no photo-carriers would be collected. That we do collect photo-carriers, means unsurprisingly that at least some of the non-idealities mentioned above must exist, so that flat-band is displaced from zero bias. Thus, depending on its sign, applied bias can either increase or decrease W and the collected photocurrent, which is in qualitative agreement with results presented Fig. 6. The simple theory suggests that W should increase as the square root of bias at sufficiently high bias, until it saturates at W_T for bias values well within our range. That Fig. 6 indicates no tendency to saturate is another indication that the theory considered is too simplified for accurate quantitative analysis. Our MOS capacitors are too poorly characterized to justify analysis by a more complete model that includes non-idealities, about which we have no definite information. At least the sign of the bias effect is in agreement with the simple model, namely positive substrate bias increases the photoresponse for n-Si and decreases it for p-type, and sufficient bias of the same sign as the conductivity type can extinguish the photoresponse entirely.

The largest photocurrent achieved in any sample with suitable bias and 0.002 times attenuation on the 0.5 mW HeNe laser with $\sim 1 \text{ mm}^2$ spot is sufficient to saturate the preamp. This photocurrent, therefore, exceeded the 10 nA preamp input limit. This allows us to estimate that the best response achieved is 10 mA/W.

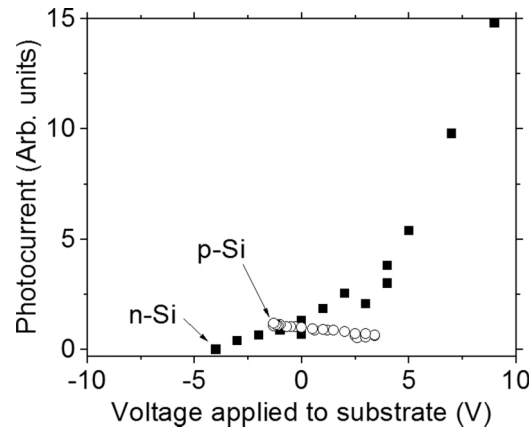


FIG. 6. Magnitude of photocurrent as a function of back-contact bias. All data are normalized to unity at zero bias.

In summary, detection of surface plasmon polaritons (SPPs) by an MOS photocapacitor was demonstrated. Dependence of the response on substrate carrier type, carrier concentration, and back-contact biasing was reported and qualitatively explained by simple MOS theory. Layer thicknesses were theoretically investigated to reveal conditions for the strongest and angularly sharpest resonant response to SPPs excited on a Kretschmann prism coupler. Electrodynamics simulations were in agreement with theory and experiment and additionally verified the field distributions expected for a Kretschmann coupler.

We note in conclusion that SPP effects are usually determined from measurements of free space optical beams, not from direct measurements of the SPP fields themselves. For example, surface plasmon resonance (SPR) biosensors based on Kretschmann couplers measure reflected light in the far field, i.e., the “R” in Fig. 1. In this paper, we have demonstrated a near-field detector placed within range of the evanescent SPP fields themselves and with only small perturbation to those fields.

Work by UCF authors was partly supported by US Air Force Research Lab Contract No. FA865013C1528 and by the Florida High Technology (I-4) program. AFRL authors were supported by Air Force Office of Scientific Research under AFOSR LRIR No. 15RYCOR162 (Program Officer Dr. Gernot Pomrenke). R.E.P. was partially supported by the AFRL Sensors Directorate. F.K.-R. acknowledges support from University of Central Florida’s research excellence fellowship and a Northrop-Grumman scholarship. C.S.W. and M.I. were also supported by the National Science Foundation under Grant No. 0955625.

¹ P. Berini, *Laser Photonics Rev.* **8**, 197 (2014).

² A. Otto, *Z. Phys.* **216**, 398 (1968).

³ C. Daboo, M. J. Baird, H. P. Hughes, N. Apsley, and M. T. Emeny, *Thin Solid Films* **201**, 9 (1991).

⁴ E. Kretschmann, *Z. Phys.* **241**, 313 (1971).

⁵ C. W. Smith, D. Maukonen, R. E. Peale, C. J. Fredrickson, M. Ishigami, and J. W. Cleary, *Proc. SPIE* **9083**, 90832Q (2014).

⁶ F. Khalilzadeh-Rezaie, R. E. Peale, D. Panjwani, C. W. Smith, J. Nath, M. Lodge, M. Ishigami, N. Nader, S. Vangala, M. Yannuzzi, and J. W. Cleary, *Proc. SPIE* **9617**, 96170E (2015).

⁷ J. W. Cleary, G. Medhi, R. E. Peale, and W. R. Buchwald, *Appl. Opt.* **49**, 3102 (2010).

⁸ J. W. Cleary, R. E. Peale, D. J. Shelton, G. D. Boreman, C. W. Smith, M. Ishigami, R. Soref, A. Drehman, and W. R. Buchwald, *J. Opt. Soc. Am. B* **27**, 730 (2010).

⁹ J. W. Cleary, G. Medhi, M. Shahzad, I. Rezadad, D. Maukonen, R. E. Peale, G. D. Boreman, S. Wentzell, and W. R. Buchwald, *Opt. Express* **20**, 2693 (2012).

¹⁰ M. Shahzad, G. Medhi, R. E. Peale, W. R. Buchwald, J. W. Cleary, R. Soref, G. D. Boreman, and O. Edwards, *J. Appl. Phys.* **11**, 123105 (2011).

¹¹ F. Khalilzadeh-Rezaie, C. W. Smith, J. Nath, N. Nader, M. Shahzad, J. W. Cleary, I. Avrutsky, and R. E. Peale, *J. Nanophotonics* **9**, 093792 (2015).

¹² J. W. Cleary, W. H. Streyer, N. Nader, S. Vangala, I. Avrutsky, B. Claffin, J. Hendrickson, D. Wasserman, R. E. Peale, and W. R. Buchwald, *Opt. Express* **23**, 3316 (2015).

¹³ F. Khalilzadeh-Rezaie, I. O. Oladeji, J. W. Cleary, N. Nader, J. Nath, I. Rezadad, and R. E. Peale, *Opt. Mat. Express* **5**, 2184 (2015).

- ¹⁴ L. D. Landau, E. M. Lifshitz, and L. P. Pitaevskii, *Electrodynamics of Continuous Media*, 2nd ed. (Butterworth-Heinemann, Oxford, 1984), Section 86.
- ¹⁵ *Handbook of Optical Constants of Solids*, edited by E. D. Palik (Academic Press, San Diego, 1985), p. 294, 356, 565, and 760.
- ¹⁶ See http://www.schott.com/advanced_optics/english/abbe_datasheets/schott-datasheet-n-bk7htl.pdf for BK7 permittivity data (last accessed May 27, 2016).
- ¹⁷ J. Nath, E. Smith, D. Maukonen, and R. E. Peale, *J. Appl. Phys.* **115**, 193103 (2014).
- ¹⁸ R. F. Pierret, *Semiconductor Device Fundamentals* (Addison-Wesley, Reading, 1996), pp. 563–600.